Research in Astronomy and Astrophysics, 25:035023 (6pp), 2025 March

https://doi.org/10.1088/1674-4527/adbea2
CSTR: 32081.14.RAA.adbea2

Detection of the Activity of 468861 (2013 LU28)

Xiao-Meng Xu[1,2,3], Xi-Liang Zhang[3], Yun-Zhao Wu[1,4], and Xiang-Yu Fan[3,5]
[1] Purple Mountain Observatory, Chinese Academy of Sciences, Nanjing 210023, China; xmxu@pmo.ac.cn
[2] School of Astronomy and Space Science, University of Science and Technology of China, Hefei 230026, China
[3] Yunnan Observatories, Chinese Academy of Sciences, Kunming 650216, China; Zhangxiliang@ynao.ac.cn
[4] State Key Laboratory of Lunar and Planetary Sciences, Macau University of Science and Technology, Macau 999078, China
[5] University of Chinese Academy of Sciences, Beijing 100049, China
Received 2024 September 8; revised 2025 February 14; accepted 2025 February 28; published 2025 March 28

Abstract

The perihelion of long-period comets places them near the Sun so they may exhibit activity. Before 2013 LU28 reached its perihelion, we performed a continuous observation to detect possible activity. Using the Lijiang 2.4 m telescope with a Johnson R filter, we measured the brightness of 2013 LU28 from 2024 January 3 to April 13. The instrumental magnitudes were subsequently transformed into the Pan-STARRS r system. Due to the noticeable descending trend in the absolute magnitude, we verified the cometary activity and constrained some photometric properties of 2013 LU28. Consequently, the increased cross-sectional area had a rate of 42.8 km^2 day^{-1}, and the corresponding mass-loss rate was 2.64 kg s^{-1} with the assumption of a dust-particle size $\bar{a} = 10\ \mu$m and the density $\rho = 400$ kg m^{-3}. We estimated the nucleus radius as $0.11 \lesssim r_n \lesssim 0.21$ km for CO sublimation and $0.20 \lesssim r_n \lesssim 0.71$ km for CO_2 sublimation and the grain size of 2013 LU28 was $a_c \simeq 117.95\ \mu$m for CO and $a_c \simeq 7.57\ \mu$m for CO_2. The long-term observations provided in this paper will offer significant value for investigating the mechanisms driving the activity of 2013 LU28.

Key words: Kuiper Belt objects: individual (2013 LU28) – techniques: photometric – minor planets, asteroids: individual (2013 LU28)

1. Introduction

Trans-Neptunian objects (TNOs) belong to the most primitive small bodies in the solar system. Research on their physical properties and surface constituents offers valuable insights into the formation and evolution of the solar system and planetary disks. Developments of deep all-sky surveys and new space-based telescopes, such as the Outer Solar System Origins Survey (OSSOS; Bannister et al. 2018) and the James Webb Space Telescope (JWST; Gardner et al. 2006), have provided more opportunities to examine volatiles and search for activity. Detecting the activity in very distant comets, especially those that never enter the water-sublimation zone ($r = 5$–6 au), will greatly improve our understanding of the triggers of activity.

(468861) 2013 LU28 is a particular object with a highly eccentric orbit. It has the orbit of a long-period comet (LPC), and the orbital parameters are as follows: semimajor axis $a = 184.2$ au, inclination $i = 125.^{\circ}3$, eccentricity $e = 0.953$, aphelion distance $Q = 359.8$ au, perihelion distance $q = 8.743$ au and an orbital period $P = 2501$ yr. The perihelion of 2013 LU28 places it within the Centaur region, hence the object is further categorized as an "extended Centaur." The diameter of 2013 LU28 was under discussion. The diameter obtained by de la Fuente Marcos & de la Fuente Marcos (2014) was between 50 and 150 km, corresponding to an absolute magnitude of 8.1 mag. After that, Hromakina et al. (2021) determined a fainter absolute magnitude of 8.6 mag using the formalism by Bowell et al. (1989), and derived the diameter in the 80-127 km range. Different from this, Slemp et al. (2022) fitted the nucleus light curve to the Pan-STARRS data and determined a radius to be ~55.7 km with an assumed albedo of 0.04. Owing to the observational constraints on distant small objects, the estimated diameters could be imprecise and exhibit a certain degree of variability. This variability may arise from complex factors such as observational geometry, viewing angles, and the overall shape and surface properties of the small bodies.

There were several studies based on photometric observations, discussing the orbital evolution and physical properties of this unique object. de la Fuente Marcos & de la Fuente Marcos (2014) used a numerical model to study the dynamical evolution of 2013 LU28, which was to be the first identified retrograde co-orbital candidate of Uranus (a quasi-satellite) and a new arrival from the trans-Neptunian region such as the Oort cloud. Hromakina et al. (2021) studied the surface properties of 2013 LU28 and discovered that it had slightly reddish surfaces, which appeared common for high-inclination asteroids.

Furthermore, Lorenzi et al. (2023) presented a set of visible and near-infrared (NIR) spectra of 2013 LU28 collected at the Telescopio Nazionale Galileo (TNG), and they found that all the visible spectra seemed to be featureless and there was an

Table 1
Specifications of the YFOSC Instrument Affiliated with the Lijiang 2.4 m Telescope

Camera	Size of CCD (pixels)	F-length[a] (mm)	FOV[b] (arcmin)	Size of pixel[c] (μm) (arcsec)
YFOSC	2148 × 2200	9840	10.1 × 10.4	13.5 × 13.5 0.283

Notes.
[a] The system's focal length
[b] The field of view
[c] A pixel's size in both μm and arcsec.

absorption at 2.02 μm due to H_2O ice in all the NIR spectra. They also suggested that the spectra of 2013 LU28 showed similarities with the spectra of Damocloids, which are solar system objects that share orbital characteristics with Halley-type and long-period comets but exhibit no visible signs of outgassing (Jewitt 2005). This proposal was soon confirmed by De Prá et al. (2024), and they also reported that the infrared spectrum of 2013 LU28 obtained with JWST showed absorption features of CO_2.

Since being discovered by the Mt. Lemmon Survey (Bressi et al. 2013) on 2013 June 8, 2013 LU28 has never been found to be active. Although there was no clear evidence of dust coma in deep stacked images, Slemp et al. (2022) suggested the possible activity of 2013 LU28 as it became brighter at a heliocentric distance between 17 and 13 au, which can be attributed to outgassing from the buried CO or CO_2. Recently, 2013 LU28 passed its perihelion ($q = 8.743$ au) on 2024 June 20, which offers a unique opportunity to study an object that has experienced minimal alteration of its surface during the age of the Solar System (Sheppard 2010) and to investigate the origin and evolution of the Outer Solar System. In this paper, we will show the results of 2013 LU28 about its mass-loss rate, nucleus radius, sublimation model and grain size based on observations conducted from 2024 January 3 to 2024 April 13, aiming to further confirm volatile activity in 2013 LU28.

2. Observations

At longitude E100°01′51.″6, latitude N26°42′33.″1, Yunnan Observatories' Lijiang 2.4 m telescope is located at a height of 3250 m. Equipped with a planetary tracking system and the Yunnan Faint Object Spectrograph and Camera (YFOSC), the Lijiang 2.4 m telescope provides robust systems to detect faint and rapidly moving objects; furthermore, the position of the telescope allows for continuous observation of 2013 LU28 as it approaches the perihelion. The details of the YFOSC instrument are presented in Table 1.

Between 2024 January 3 and April 13, 43 images of 2013 LU28 were obtained over six nights using the YFOSC and the Johnson R filter on the Lijiang 2.4 m telescope. To improve the signal-to-noise ratio of 2013 LU28, the tracking mode for a planet was selected, with the tracking rates in R.A. and decl. calculated by the Minor Planet Center (MPC) of the International Astronomical Union (IAU). Additionally, the images were scaled to 0.566 arcsec pixel^{-1} using 2 × 2 binning. The exposure times of individual images varied between 90 and 120 s based on the object's brightness.

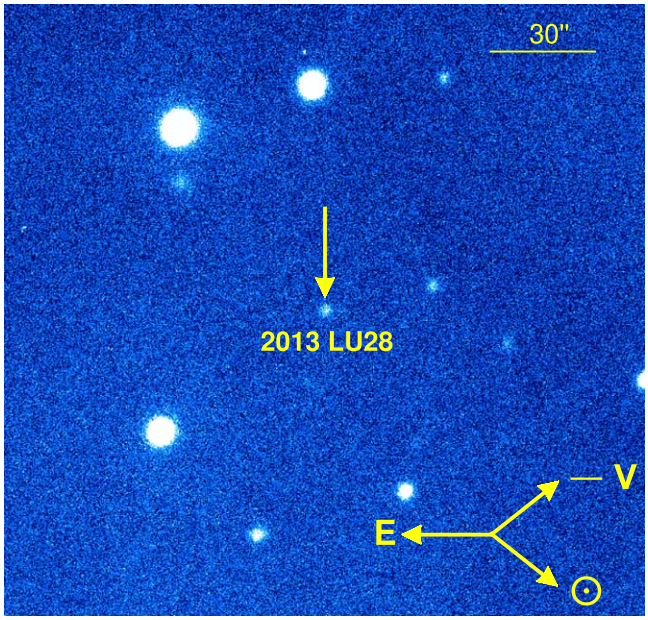

Figure 1. An image of 2013 LU28 taken on UT 2024 February 27 at $r_H = 8.767$ au, with size of 170″ × 170″. The negative heliocentric velocity vector ($-V$) of 2013 LU28, the east direction (E) and the positive solar vector ($\odot$) are marked, with north at the top.

3. Data Reduction

The photometric observations were analyzed using the routine processes with the Image Reduction and Analysis Facility (IRAF, Tody 1986). Before measuring the brightness of 2013 LU28, we first corrected the effects of bias and flat field. An image of 2013 LU28 observed on UT 2024 February 27 at a heliocentric distance of $r_H = 8.767$ au is displayed in Figure 1.

With an aperture 4.″2 in radius, the field stars and brightness of 2013 LU28 for all observations were measured, and we used the Panoramic Survey Telescope and Rapid Response System 1 (PS1) catalog to adjust the brightness. PS1 data of field stars were then transformed to the UBVRI broad band photometric system, and Kostov & Bonev (2018) were referenced to convert the Pan-STARRS r values to Stetson R. The formula is as follows:

$$\begin{aligned} R - r &= C_0 + C_1 \times (g - r) R - r \\ &= D_0 + D_1 \times (g - r) + D_2 \times (g - r)^2, \end{aligned} \quad (1)$$

Table 2
Photometric Information and Absolute Magnitudes of 2013 LU28

UT Date	MJD[a]	Δ[b] (au)	r_H[b] (au)	α[b] (deg)	$H \pm \sigma$[c]
2024-01-03	60312.740	7.984	8.795	3.8	8.244 ± 0.02
2024-01-17	60326.685	7.933	8.787	3.4	8.215 ± 0.02
2024-01-30	60339.752	7.942	8.780	3.6	8.168 ± 0.02
2024-02-09	60349.643	7.985	8.775	4.0	8.134 ± 0.02
2024-02-27	60367.689	8.137	8.767	5.2	8.094 ± 0.05
2024-04-13	60413.679	8.795	8.752	6.5	8.036 ± 0.02

Notes.
[a] Modified Julian Date.
[b] Geocentric distance Δ (au), heliocentric distance r_H (au) and phase angle (degree).
[c] Average absolute magnitude and errors of 2013 LU28.

$$R - r = C_0 + C_1 \times (r - i) R - r = D_0 + D_1 \times (r - i) + D_2 \times (r - i)^2, \quad (2)$$

where C_0, C_1, D_0 and D_1 are the coefficients and derived from fits (see Table 2 in Kostov & Bonev (2018)). After obtaining the transformed magnitudes R, we apply a linear fit to the data and derived the slope S and zero-point Z. The relationship between instrumental magnitudes $m_{\rm inst}$ and those calculated m' by using the transformations can be represented by the following formula

$$m_{\rm inst} = Z + S \times m'. \quad (3)$$

Applying the derived slope and zero-point, the standard magnitude $m_{\rm calculated}$ of 2013 LU28 is calculated as

$$m_{\rm calculated} = (m_{\rm inst} - Z)/S. \quad (4)$$

Afterward, we can derive the absolute magnitude of 2013 LU28 by correcting for the effects of geocentric and heliocentric distances and the phase angle, according to formulas (5) and (6)

$$H = R - 5\log_{10}(r_H \Delta) - g(\alpha), \quad (5)$$

$$g(\alpha) = 0.04\alpha, \quad (6)$$

where the absolute magnitude is denoted by H, while Δ and r_H represent geocentric and heliocentric distances of 2013 LU28, respectively. The term $g(\alpha)$ accounts for phase darkening (For most comets, the phase coefficients are typically low as a response to their low albedo, with a value of 0.04 mag per degree commonly used in research about active comets; e.g., Jewitt & Meech 1987; Alvarez-Candal et al. 2016; Zhang et al. 2019; Jewitt et al. 2017; but note that the value of $g(\alpha)$ is not critical because the phase angles are small.), with α being the phase angle. The observational details and mean absolute magnitude of 2013 LU28 are presented in Table 2 for each night. In Figure 2, all absolute magnitudes are shown as black dots, with their corresponding errors indicated by uncertainty bars, and the linear fitting analysis of the brightness variation indicates a decreasing trend in magnitude. Furthermore, the plot of the true anomaly versus absolute magnitude for 2013 LU28, presented in Figure 3, demonstrates an increase in absolute magnitude between TA $= -100^\circ$ to -50°, and a subsequent decrease for TA $= -10^\circ$ to 0°, which confirms the ongoing activity of the object.

4. Discussion

4.1. Mass-loss Rate

The absolute magnitude of an inactive asteroid should remain relatively stable. However, Table 2 and Figure 2 reveal an apparent declining trend in the absolute magnitudes of 2013 LU28, which implies significant evidence of possible activity. The brightness corresponds to a large rise in the scattering cross-section, which is induced by the mass loss in the form of dust. Therefore, we have calculated the effective cross-section and mass-loss rate based on the formula for cometary activity.

Given the limited studies on 2013 LU28, its model parameters have not been definitively determined. Nonetheless, we can estimate these parameters using nominal parameters observed for other comets, both in situ and from ground-based observations (Meech et al. 2017a; Zhang et al. 2019). We assume the following: the geometric albedo $P_v = 0.04$, the average radius of a dust grain $\bar{a} = 10$ μm and bulk density $\rho_d = 400\,{\rm kg\ m^{-3}}$.

We calculated the effective scattering cross-section of 2013 LU28 using the relation between the scattering cross-section and absolute magnitude as follows (Jewitt et al. 2017)

$$C_d = \frac{1.5 \times 10^6}{P_v} 10^{-0.4H}, \quad (7)$$

where P_v is an assumption of the geometric albedo and the unit of C_d is km^2. The effective scattering cross-sections of 2013 LU28 observed with the Lijiang 2.4 m telescope from 2024 January 3 and 2024 April 13 are detailed in Table 3, showing an obvious increase trend.

We estimated the mean mass-loss rate of the comet, represented as $\bar{\dot{M}}$, using this formula (Jewitt et al. 2017)

$$\bar{\dot{M}} = \frac{4\rho_d \bar{a}}{3} dC_d/dt, \quad (8)$$

and with the assumed parameters, we computed the mean mass-loss rate dM/dt of 2013 LU28 to be approximately $2.64\,{\rm kg\ s^{-1}}$, as shown in Table 4 along with the increasing rates of scattering cross-section dC_d/dt. The uncertainty accounted for both the photometric error and the albedo error. The mass-loss rate in our calculation was larger than those calculated by Slemp et al. (2022), which had a gas production rate ranging from $1.1\,{\rm kg\ s^{-1}}$ for CO to $1.5\,{\rm kg\ s^{-1}}$ for CO_2. The main reason may be the difference in heliocentric distance at the time of observation. (In our calculation, r_H was between 8.752–8.795 au, while they have r_H between 14.7–17.1 au.) Choosing different mean radius of the

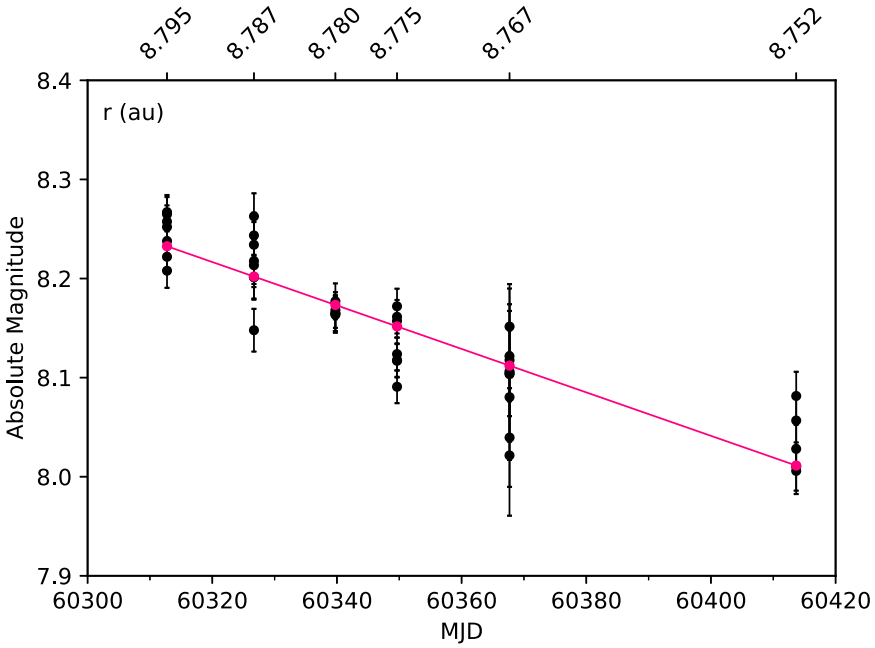

Figure 2. Observed (black) and fitted (red) absolute magnitudes of 2013 LU28.

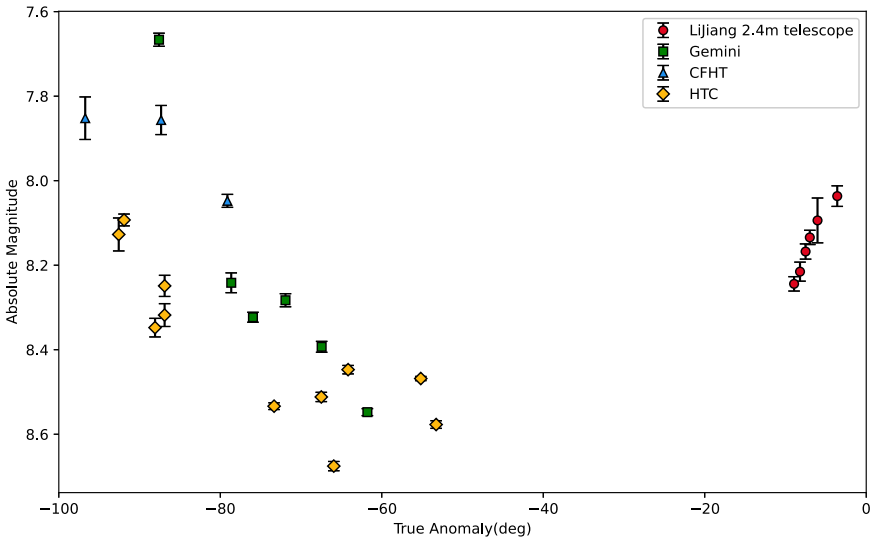

Figure 3. The true anomaly and absolute magnitude of 2013 LU28 with different telescopic observations.

dust grains and using different calculation methods are also reasonable factors.

Some distant objects showing no activity may turn out to be active at large distances, while some others exhibit cometary activity as they approach the perihelion. There were some recorded mass-loss rates of these objects; for instance, Comet C/2002 VQ94 was active near 8.36 au with dust mass-loss rate between 10 and 20 kg s^{-1} (Korsun et al. 2014). The activity of the long-period Comet C/2015 ER61 was reported by Meech et al. (2017b), which initially appeared inactive, and the subsequent activity was driven by CO or CO_2 with the CO_2 production rate being 6.139 kg s^{-1}. Comet C/2017 K2 was driven by CO (Meech et al. 2017a) and when it reached perihelion, the mass-loss rate peaked at 127 kg s^{-1} (Zhang et al. 2019).

4.2. Size of Nucleus

The sublimation of a supervolatile ice, such as CO, CO_2, O_2 or N_2, as suggested by Jewitt et al. (2017), could potentially

Table 3
Cross-sections of 2013 LU28

UT Date	MJD [a]	$C_d \pm \sigma(10^4\ \mathrm{km}^2)$[b]
2024-01-03	60312.740	1.89 ± 0.01
2024-01-17	60326.685	1.94 ± 0.02
2024-01-30	60339.752	2.03 ± 0.01
2024-02-09	60349.643	2.09 ± 0.01
2024-02-27	60367.689	2.17 ± 0.05
2024-04-13	60413.679	2.29 ± 0.02

Notes.
[a] Modified Julian Date.
[b] Cross-sections and errors of 2013 LU28.

Table 4
Rates of Variation of Scattering Cross-section and Mean Mass Loss of 2013 LU28

dC_d/dt ($\mathrm{km}^2\mathrm{day}^{-1}$)	$\bar{M}$ ($\mathrm{km\ s}^{-1}$)
42.8 ± 3.2	2.64 ± 0.20

propel the activity of remote comets. Given the abundance in the outer solar system, these volatiles are likely to be prevalent on objects exhibiting long-period comet orbits. Additionally, comets can create outgassing owing to these molecules, which ejects dust particles from the nucleus' surface and subsurface. This phenomenon becomes observable at diverse heliocentric distances, depending on factors such as the dust grain sizes, the nucleus's surface temperature and the latent heat of sublimation (Meech & Svoren 2004).

By employing the empirical equilibrium equation linking temperature for particles, heliocentric distance and activity, we may determine the mass flux of the sublimated volatiles and the nucleus's size. In this equation,

$$\frac{L_\odot}{4\pi r_H}(1-A)\cos\xi = \epsilon\sigma T^4 + L(T)f_s(T), \tag{9}$$

A denotes the Bond albedo, r_H (m) is the heliocentric distance of 2013 LU28, $L_\odot$ (W) represents the luminosity of the Sun, and $\cos\xi$ is the effective projection factor. The temperatures of the isothermal sphere and subsolar point are represented by $\cos\xi = 1/4$ and 1, respectively. The emissivity of 2013 LU28 is expressed by ϵ, the Stefan-Boltzmann constant is represented as $\sigma = 5.67 \times 10^{-8}$ ($\mathrm{W\ m}^{-2}\ \mathrm{K}^{-4}$), the surface temperature is T(K), the latent heat is L(T) ($\mathrm{J\ kg}^{-1}$), and $f_s(T)$ ($\mathrm{kg\ m}^{-2}\ \mathrm{s}^{-1}$) represents the mass flux of sublimated ice, where the lower and upper limits are provided by isothermal and subsolar sublimation, respectively. We solved Equation (5) using the ice thermodynamic parameters from Prialnik et al. (2004) and Cowan & A'Hearn (1979), assuming $A = 0.04$ and $\epsilon = 0.9$. Considering that the variation of 2013 LU28's r_h was negligible during the observation period, we adopted $r_h = 8.767$ on 2024 February 27 for this calculation. The obtained results indicate that the mass flux for CO sublimation ranges from 1.86×10^{-5} to 7.47×10^{-5} $\mathrm{kg\ m}^{-2}\ \mathrm{s}^{-1}$, while that for CO_2 sublimation ranges from 1.67×10^{-6} to 2.12×10^{-5} $\mathrm{kg\ m}^{-2}\ \mathrm{s}^{-1}$. Presented in Table 5 are the calculations of the surface area $A_s = dM/dtf_s^{-1}$, which is required to sustain the activity of 2013 LU28, as well as the range of the nucleus radius r_n, which refers to the size of a bare nucleus with one type of volatile ice that could sustain the observed rate of corresponding gas sublimation. Compared with Slemp et al. (2022), we have confined the size of the nucleus to a narrower range.

Table 5
Surface Area $A_s = \bar{M}/f_s$ and Radius Range of the Nucleus r_n for 2013 LU28

Ices	CO	CO_2
$A_s(\mathrm{km}^2)$	$0.04 \lesssim A_s \lesssim 0.14$	$0.12 \lesssim A_s \lesssim 1.58$
r_n(km)	$0.11 \lesssim r_n \lesssim 0.21$	$0.20 \lesssim r_n \lesssim 0.71$

4.3. Size of a Grain

It is possible to approximate the critical grain size a_c that could be dragged from the nucleus using the gas-drag force $F_D = C_D\pi a^2 \mu m_\mathrm{H} N v_\mathrm{th}^2$, where $m_\mathrm{H} = 1.67 \times 10^{-27}$ kg is the mass of a hydrogen atom, C_D is the dimensionless drag coefficient, μ denotes the molecular weight ($\mu = 28$ for CO and $\mu = 44$ for CO_2), N stands for the number density of the molecule, and v_th is the gas's thermal speed. Using the surface temperature T (K) (see Table 1 in Meech & Svoren 2004) and nucleus size r_n of 2013 LU28 derived earlier, we can estimate the critical dust particle size applying the equation proposed by Hui et al. (2017). By balancing the surface's gravitational force with the gas-drag force and neglecting the object's rotation, Hui et al. (2017) derive the formula

$$a_c = \frac{9C_D\bar{M}}{32\pi^2 G\rho\rho_d r_n^3}\sqrt{\frac{2k_B T}{\pi\mu m_\mathrm{H}}}, \tag{10}$$

where $k_\mathrm{B} = 1.38 \times 10^{-23}$ $\mathrm{J\ K}^{-1}$ is the Boltzmann constant, $G = 6.67 \times 10^{-11}$ $\mathrm{m}^3\ \mathrm{kg}^{-1}\ \mathrm{s}^{-2}$ denotes the gravitational constant, ρ represents the density of the nucleus, and r_n is related to the median value (for CO, $r_n = 0.16$ km; for CO_2, $r_n = 0.45$ km). Under the assumption of a gas-to-dust production ratio of unity, with $\rho = \rho_d$ and $C_D = 1$, we give $a_c \simeq 117.95$ μm for CO sublimation and $a_c \simeq 7.57$ μm for CO_2 using Equation (10), consistent with results by Slemp et al. (2022). Considering the dust model's average dust size of $\bar{a} = 10$ μm, we favor the situation such that CO_2 and CO both affect the critical particle size, with CO_2 (and other volatile substances) playing a dominant role. It appears probable that the activity is triggered by subsurface CO ice's sublimation, since surface CO ice would remain active at far greater distance from the Sun (120 au).

5. Summary

We observed 2013 LU28 before it reached perihelion with the Lijiang 2.4 m telescope over three months. The summary of this research is presented here.

(i) The scattering cross-section's increased rate, approximately 42.8 km^2 day^{-1}, indicates that the activity of 2013 LU28 was stable during our observations.

(ii) Assuming a geometric albedo of 2013 LU28 $p_v = 0.04$, a density of $\rho = 400$ kg m^{-3} and a mean particle size of $\bar{a} = 10$ μm, we calculated the mass-loss rate of 2013 LU28 to be $\bar{\dot{M}} = 2.64 \pm 0.20$ kg s^{-1}.

(iii) According to these observations, the size of the nucleus corresponding to the amount of ice sublimation was derived as $0.11 \lesssim r_n \lesssim 0.21$ km for CO sublimation and $0.20 \lesssim r_n \lesssim 0.71$ km for CO_2 sublimation.

(iv) The estimated grain size of 2013 LU28 is $a_c \simeq 117.95\mu$m for CO sublimation and $a_c \simeq 7.57\mu$m for CO_2 sublimation. Therefore, we conclude that CO and CO_2 both contribute to the activity of 2013 LU28 during our observation and CO_2 is the main driver of the activity.

In conclusion, further observations are needed to explore the physical properties and activity. We will proceed with observing 2013 LU28, aiming to refine its photometric and spectral properties using the Lijiang 2.4 m telescope and the newly launched JWST.

Acknowledgments

We thank Bin Yang and Liang Liang Yu for giving suggestions so generously. We also thank the anonymous referee for their helpful comments. We acknowledge the support of the staff of the Lijiang 2.4 m telescope, which is jointly operated and administrated by Yunnan Observatories and the Center for Astronomical Mega-Science, Chinese Academy of Sciences. Funding for the telescope has been provided by CAS and the People's Government of Yunnan Province. This work was funded by the Civil Aerospace pre-research project D020302, National Natural Science Foundation of China (U12150009, 12150009), and the CAS Light of West China Program. We also acknowledge the science research grants from the China Manned Space Project with NO.CMS-CSST-2021-B10.

ORCID iDs

Yun-Zhao Wu https://orcid.org/0000-0001-8408-1204

References

Alvarez-Candal, A., Pinilla-Alonso, N., Ortiz, J. L., et al. 2016, A&A, 586, A155
Bannister, M. T., Gladman, B. J., Kavelaars, J. J., et al. 2018, ApJS, 236, 18
Bowell, E., Hapke, B., Domingue, D., et al. 1989, in Asteroids II, ed. R. P. Binzel, T. Gehrels, & M. S. Matthews (Tucson: AZ: Univ. Arizona Press), 524
Bressi, T. H., Mastaler, R. A., Schwartz, M., et al. 2013, MPEC, 2013-V72, L69
Cowan, J. J., & A'Hearn, M. F. 1979, M&P, 21, 155
De Prá, M. N., Hénault, E., Pinilla-Alonso, N., et al. 2024, NatAs, 10, 252
de la Fuente Marcos, C., & de la Fuente Marcos, R. 2014, Ap&SS, 352, 409
Gardner, J. P., Mather, J. C., Clampin, M., et al. 2006, SSRv, 123, 485
Hromakina, T., Belskaya, I., Krugly, Y., et al. 2021, A&A, 647, A71
Hui, M. T., Jewitt, D., & Clark, D. 2017, AJ, 155, 25
Jewitt, D. 2005, AJ, 129, 530
Jewitt, D., Hui, M. T., Mutchler, M., et al. 2017, ApJL, 847, L19
Jewitt, D., & Meech, K. 1987, AJ, 93, 1542
Korsun, P. P., Rousselot, P., Kulyk, I. V., et al. 2014, Icar, 232, 88
Kostov, A., & Bonev, T. 2018, BlgAJ, 28, 3
Lorenzi, V., Pinilla-Alonso, N., Licandro, J., et al. 2023, LPICo, 2851, 2379
Meech, K. J., Kleyna, J. T., Hainaut, O., et al. 2017a, ApJL, 849, L8
Meech, K. J., Schambeau, C. A., Sorli, K., et al. 2017b, AJ, 153, 206
Meech, K. J., & Svoren, J. 2004, in Comets II, ed. M. C. Festou, H. U. Keller, & H. A. Weaver (Tucson, AZ: Univ. Arizona Press/Lunar Planet. Inst), 317
Prialnik, D., Benkhoff, J., & Podolak, M. 2004, in Comets II, ed. M. C. Festou et al. (Tucson, AZ: Univ. of Arizona Press), 359
Sheppard, S. S. 2010, AJ, 139, 1394
Slemp, L. A., Meech, K. J., Bufanda, E., et al. 2022, PSJ, 3, 34
Tody, D. 1986, Proc. SPIE, 627, 733
Zhang, X. L., Jewitt, D., & Hui, M. T. 2019, MNRAS, 487, 2919